Publications of the Astronomical Society of Australia (2026), **43**, e061, 12 pages
doi:10.1017/pasa.2026.10193

CAMBRIDGE UNIVERSITY PRESS

Research Article

Two intersecting radio shells: Relics of galaxy merger shocks?

Bärbel Silvia Koribalski[1,2], Klaus Dolag[3,4], Ildar Khabibullin[3,4], Ludwig Boess[5], Anna Ivleva[3] and Ray Norris [1,2]

[1]Australia Telescope National Facility, CSIRO, Space and Astronomy, Australia, [2]Western Sydney University, Penrith South DC, NSW, Australia, [3]Universitäts-Sternwarte, Fakultät für Physik, Ludwig-Maximilians-Universität München, München, Germany, [4]Max-Planck-Institut für Astrophysik, Garching, Germany and [5]Department of Astronomy and Astrophysics, William Eckhart Research Center, The University of Chicago, Chicago, IL, USA

Abstract

We present the discovery of two intersecting radio shells, likely radio relics, surrounding a compact galaxy group dominated by a massive elliptical galaxy. The shells present as partial, edge-brightened rings with diameters of ∼240″ (∼720 kpc) each and resemble a pair of odd radio circles. The central galaxy, WISEA J184105.19–654753.8, which shows signs of interactions, is radio bright, has a stellar mass of 3.1×10^{11} $M_{\odot}$ (for a redshift of $z_{\rm phot} \sim 0.18$) and is located in the intersect region. The double radio shell system, which we refer to as ORC J1841–6547, also known as ORC 6, was detected in 944 MHz radio continuum images obtained with Phased Array Feeds on the Australian Square Kilometre Array Pathfinder (ASKAP). The more prominent, north-western shell may be associated with an X-ray detection, while the weaker, south-eastern shell has no counterpart at non-radio wavelength. We propose outwards moving shocks from galaxy mergers driving into the intragroup medium, re-energising relic radio lobes, as a possible formation scenario for the observed radio shells. We conclude that at least some ORCs are shock-energised relics in the outskirts of galaxy groups, which originate during the merger evolution of the brightest group galaxy.

Keywords: Galaxies: evolution; galaxies: groups: general; radio continuum: galaxies

(Received 15 July 2025; revised 28 February 2026; accepted 8 April 2026)

1. Introduction

Extended, steep-spectrum radio sources of low surface brightness (LSB), not directly associated with a galaxy, were first discovered in and around nearby X-ray clusters (Ballarati et al. 1981, and references therein). While initially referred to as *'halo type radio sources'*, these are now known as radio halos in the centres of galaxy clusters and radio relics in their outskirts (e.g. Ferrari et al. 2008; van Weeren et al. 2019). Already then it was noted that such diffuse radio sources are difficult to observe due to the need for high angular resolution together with high sensitivity to extended LSB emission. Today's radio interferometers are highly capable to detect such structures.

Through a combination of wide-field imaging, good resolution and sensitivity, ASKAP radio surveys covering frequencies from 700 to 1 800 MHz have become a treasure trove of findings (see highlights in Koribalski 2022), continuing to surprise and inspire new techniques to explore the vast volumes of data (Segal et al. 2023; Gupta et al. 2024, 2025). Recent discoveries of large-scale diffuse radio sources with the Australian Square Kilometre Array Pathfinder (ASKAP), such as cluster relics and halos (Brüggen et al. 2021; Venturi et al. 2022; Riseley et al. 2022; Duchesne et al. 2024; Koribalski et al. 2024b), extended radio galaxies (e.g. Gürkan et al. 2022; Velović et al. 2022; Venturi et al. 2022; Koribalski et al. 2024a; Koribalski 2026), bipolar outflows from a spiral galaxy disc (Koribalski et al. 2026), odd radio circles (Norris et al. 2021b; Koribalski et al. 2021; Koribalski et al. 2024c) and an intergalactic supernova remnant (Filipović et al. 2022), give just a glimpse of what to expect from the on-going sky surveys (e.g. Norris et al. 2011; Norris et al. 2021a; Koribalski 2012; Koribalski et al. 2020). Among the listed sources, odd radio circles (ORCs) stand out as one of the most peculiar and interesting.

The first two odd radio circles, ORC J2103–6200 and ORC J1555+2726, were discovered by Norris et al. (2021b) in ASKAP 944 MHz radio continuum data from the 'Evolutionary Map of the Universe' Pilot Survey (EMU-PS, Norris et al. 2021a) and in 325 MHz radio continuum data from the Giant Metrewave Radio Telescope (GMRT), respectively. The subsequent ASKAP discovery of another prominent radio ring, ORC J0102–2450, at $z = 0.27$ by Koribalski et al. (2021), notably the third odd radio circle with a massive elliptical galaxy ($\gtrsim 10^{11}$ $M_{\odot}$) at their respective centre, established the importance of the central host galaxies as being responsible for the radio ring/shell formation. The diameters of the above three ORCs are each around one arcminute, corresponding to physical sizes of ∼300–500 kpc at their respective host galaxy redshift of $z \sim 0.27$–0.55. As the search for ORCs continues, we only note two further ORCs recently found in MeerKAT radio continuum images: ORC J1027–4422 (Koribalski et al. 2024b) at relatively low Galactic latitude, making it difficult to study the likely host galaxy and its environment, and ORC J0219–0505 (Norris et al. 2025a) with a diameter of only 114 kpc for $z = 0.196$.

ORCs somewhat resemble (but are smaller, fainter, and more ring-like than) double radio relics in the outskirts of merging galaxy clusters (e.g. Bagchi et al. 2006; van Weeren et al. 2019; Jones et al. 2023; Koribalski et al. 2024b). Using high-resolution cosmological simulations, Dolag et al. (2023) find that ORCs occasionally result from outwards moving merger shocks during

Corresponding author: Bärbel Silvia Koribalski; Email: baerbel.koribalski@csiro.au.

Cite this article: Koribalski BS, Dolag K, Khabibullin I, Boess L, Ivleva A and Norris R. (2026) Two intersecting radio shells: Relics of galaxy merger shocks?. *Publications of the Astronomical Society of Australia* **43**, e061, 1–12. https://doi.org/10.1017/pasa.2026.10193

© The Author(s), 2026. Published by Cambridge University Press on behalf of Astronomical Society of Australia. This is an Open Access article, distributed under the terms of the Creative Commons Attribution licence (https://creativecommons.org/licenses/by/4.0/), which permits unrestricted re-use, distribution and reproduction, provided the original article is properly cited.

the evolution of the growing central elliptical galaxy in groups. This scenario can also explain the formation of two nearby radio shell systems recently found in ASKAP images – Physalis ($z = 0.017$, Koribalski et al. 2024c), and Cloverleaf ($z = 0.046$; Dolag et al. 2023, Koribalski et al. in preparation) – suggesting that ORCs are radio relics in the outskirts of galaxy groups, formed through merger shocks. The investigations by both (Koribalski et al. 2024c) and, more recently, Ivleva et al. (2026) led to the conclusion that such merger shocks must be expanding into remnant/fossil plasma from ageing radio lobes. This scenario is further explore here.

In this paper we present the discovery of ORC J1841–6547 (previously noted as ORC 6 in Dolag et al. 2023) found during the search for ORCs and other extended radio sources in a deep ∼30 deg^2 ASKAP field towards the nearby starburst galaxy NGC 6744 (HIPASS J1909–63a, Koribalski et al. 2004). A summary of the ASKAP multi-epoch observations is given in Section 2, followed by our results in Section 3, comparison with other odd radio circles and radio shell systems in Section 4, and our discussion of the new system in Section 5. Our conclusions are given in Section 6.

2. ASKAP observations and data processing

ASKAP is a powerful radio interferometer consisting of 36 × 12-m antennas, each equipped with a wide-field Phased Array Feed (PAF) operating at frequencies from 700 MHz to 1.8 GHz (Johnston et al. 2008). Its longest baselines extend to 6.4 km. For radio continuum studies the currently available bandwidth of 288 MHz is divided into 288 × 1 MHz coarse channels. A comprehensive system overview is given in Hotan et al. (2021), and science highlights are presented in Koribalski (2022).

For the radio analysis of ORC 1841–6547, we obtained three fully calibrated ASKAP 944 MHz radio continuum images from the CSIRO ASKAP Science Data Archive (CASDA).[a] All fields are centred at α, δ (J2000) = $19^{\rm h}\,08^{\rm m}\,00^{\rm s}$, $-64^\circ\,30'\,00''$, close to the nearby spiral galaxy NGC 6744 (HIPASS J1909–63a, Koribalski et al. 2004). We use scheduling blocks (SB) 32 018 (7 h), 32 039 (7 h) and 32 235 (10 h), observed in September 2021, centred at 943.5 MHz; the respective integration times are given in brackets (see also Dobie et al. 2023). The total ASKAP integration time for this field is 24 h. ASKAP PAFs were used to form 36 beams arranged in a 6 × 6 closepack36 footprint (see Hotan et al. 2021, their Figure 20), each delivering a ∼30 deg^2 field of view out to the half power point. Using rms weighting, we combined the three images after convolving each to a common 15″ resolution, achieving a sensitivity of ∼25 μJy beam^{-1} near ORC J1841–6547. Furthermore, we were able to make an ASKAP 1.4 GHz radio continuum image at 20″ resolution by combining five 1 h images from SBs 43 495, 43 530, 43 570, 43 605 and 43 695, also available in CASDA. Here the centre frequency is 1 367.5 MHz, but the bandwidth is only 144 MHz due to interference in part of the band. We measure an rms noise of ∼80 μJy beam^{-1}.

3. Results

The double-shell system, named ORC J1841–6547, was found in ASKAP 944 MHz radio continuum images and is shown in Figure 1. It consists of two overlapping, partial shells or bubbles spanning a total extent of ∼7′. The system properties are summarised in Table 1. Despite their LSB, the radio shells are well defined against their surroundings. In Figure 2 we show a high contrast radio image of ORC J1841–6547 as well as coloured overlays to trace its double-shell morphology, followed by a WISE infrared image overlaid with ASKAP contours in Figure 3. More details are given in Section 3.1.

Within the shell intersect region we note three adjacent radio sources. Of these, the compact, central radio source is associated with the elliptical galaxy WISEA J184105.19–654753.8. This is the likely host galaxy of ORC J1841–6547 with a photometric redshift of ∼0.18 (Wen & Han 2024), depicted in Figures 4 and 5. More details are presented in Section 3.2. The two extended radio sources SW of the host are discussed in Section 3.3, followed by a study of the system's potential X-ray emission in Section 3.4.

3.1. The radio shell emission

The stunning double ring radio morphology of ORC J1841–6547 consists of a near-complete (primary) ring centred ∼60″ NW of the central radio source, associated with a massive elliptical galaxy discussed in the next section, and a partial (secondary) ring, centred ∼90″ SE of the host. The NW ring has only a small gap towards the south-east, while only half of the SE ring is currently detected (see Figure 2). The outer ring diameters are well defined (each ∼240″ in size), seen in clear contrast against the surrounding image noise. Some ring segments appear to be very narrow (not resolved by the 15″ ASKAP synthesised beam), while other segments are more diffuse and much wider than the beam. Fitting a polynomial to the NW ring profile gives a mean ring width of 20″.

Figure 2 shows a high contrast ASKAP radio continuum image of the ORC J1841–6547, overlaid with two rings (middle panel) and two partial, slightly elliptical segments ($PA \approx 45^\circ$, right panel) following the brightest radio emission. Figure 3 shows the ASKAP radio contours overlaid onto a WISE colour-composite image. Both rings are likely radio shells or bubbles where the diffuse emission detected inside their outer rims is mainly from the curved shell surface seen in projection. We look into several formation mechanisms in Section 4.

The total ASKAP 944 MHz flux density, $S_{944\,\rm MHz}$, of the system is 17.5 ± 0.5 mJy. This includes 3.2 ± 0.2 mJy from the central region shown in Figure 4, encompassing the radio source associated with the host galaxy and the south-western extension, as well as 0.9 mJy from the radio-bright background galaxy (WISEA J184045.77–654653.2) located within the NW ring. This means we detect ∼13.6 mJy in the radio shells alone, which gives a radio power of $P_{944\,\rm MHz} = 4\,\pi\,D_{\rm L}^2 S_{944\,\rm MHz} = 1.2 \times 10^{24}$ W Hz^{-1} for $D_{\rm L} = 872$ Mpc (for $S_\nu \propto \nu^\alpha$).

The 2′-resolution GLEAM 200 MHz images (Hurley-Walker et al. 2017), which typically have a 5σ detection threshold of 50 mJy beam^{-1}, do not allow a flux estimate due to confusion. We calculate expected 200 MHz shell fluxes of ∼65, ∼300 and ∼1 500 mJy for $\alpha = -1$, −2 and −3, respectively.

The ASKAP 1.4 GHz images of ORC 6 are very noisy compared to those at 944 MHz, which means that our 1.4 GHz flux estimates are very uncertain. By integrating over the area detected at 944 MHz we measure a 1.4 GHz flux of ∼6 mJy corresponding to a radio power of $P_{1.4\rm GHz} = 5.5 \times 10^{23}$ W Hz^{-1}. This includes the core, the wedge-shaped emission and the radio shells. The latter have a total flux of ∼4.0 mJy ($P_{1.4\,\rm GHz} = 3.8 \times 10^{23}$ W Hz^{-1}), which

[a]CASDA: https://data.csiro.au/domain/casdaObservation.

https://doi.org/10.1017/pasa.2026.10193 Published online by Cambridge University Press

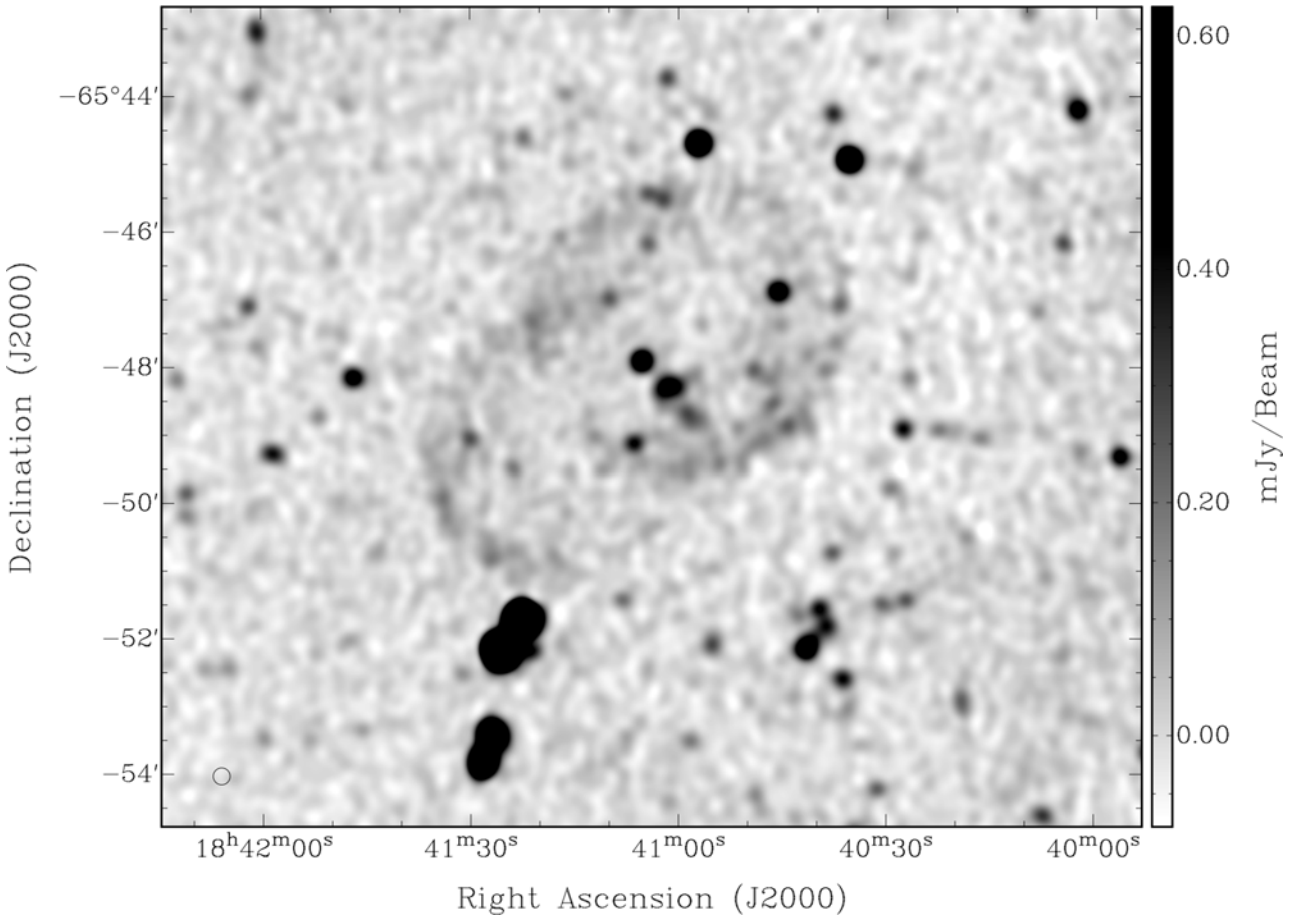


Figure 1. Deep (24 h) ASKAP 944 MHz radio continuum image of the double-shell system ORC J1841–6547 (also known as ORC 6). The image resolution (15") is indicated in the bottom left corner.

Table 1. Properties of ORC J1841–6547.

Radio morphology	Double shell system
Radio core position	
α, δ (J2000)	$18^h\ 41^m\ 05^s.16$, −65° 47' 54.6
Galactic l,b	329.5°, −23.5°
Radio core flux	1.13 mJy (944 MHz)
	0.75 mJy (1 368 MHz)
Host galaxy name	WISEA J184105.19–654753.8
Host galaxy redshift	∼0.18 (see Table 2)
Radio shell diameter	∼240″ (0.73 Mpc)
Radio system size	∼420″ (1.27 Mpc)
Radio shell flux	14.3 mJy (944 MHz)
	6.0 mJy (1368 MHz)
Environment	Compact galaxy group

suggests a steep spectral index of $\alpha \sim -3$. We discuss potentially associated X-ray emission in Section 3.4.

3.2. The host galaxy and its environment

The central, compact radio source in the intersect of the double shell system is associated with the elliptical galaxy WISE J184105.19–654753.8 (see Figure 4). This is the likely host galaxy of ORC J1841–6547. Its radio flux density is 1.13 mJy at 944 MHz and 0.75 mJy at 1.4 GHz, resulting in a spectral index of $\alpha = -1.1$ for $S_\nu \propto \nu^\alpha$ (see Table 4). A summary of the galaxy properties is given in Table 2. Its classification as an elliptical galaxy is based on both the galaxy's optical appearance in the DESI Legacy Survey images (Dey et al. 2019) and its location in the WISE colour-colour diagram (see Jarrett et al. 2017). From its 2MASS K_s-band luminosity we estimate a black hole (BH) mass of $\sim 4 \times 10^8$ M$_\odot$, following Graham (2007). For the host galaxy, WISE J184105.19–654753.8, (Wen & Han 2024, hereafter WH24) estimate a photometric redshift of 0.18, based on DESI Legacy Survey images (Dey et al. 2019), and derive a stellar mass of $\log M_\star = 11.5$. Examining the redshift catalogue by WH24 we find three likely companion galaxies (listed in Table 3), establishing the ORC host galaxy as the brightest galaxy of a compact group. An envelope of diffuse light, spanning at least 30″ (70–90 kpc, see Figure 5) surrounds the host galaxy and its closest companion (c1), indicating tidal interaction and/or merger activity. WH24 note that WISE J184105.19–654753.8 has the attributes of a brightest cluster galaxy (BCG). They give a cluster membership of 12 galaxies, a radius of $R_{500c} = 0.6$ Mpc and a mass of $M_{500c} = 0.75 \times 10^{14}$ M$_\odot$ (both for the enclosed overdensity 500 times larger than the critical density of the Universe). The location of ORC J1841–6547 in the radio power versus total mass diagram, shown by (Koribalski et al.

https://doi.org/10.1017/pasa.2026.10193 Published online by Cambridge University Press

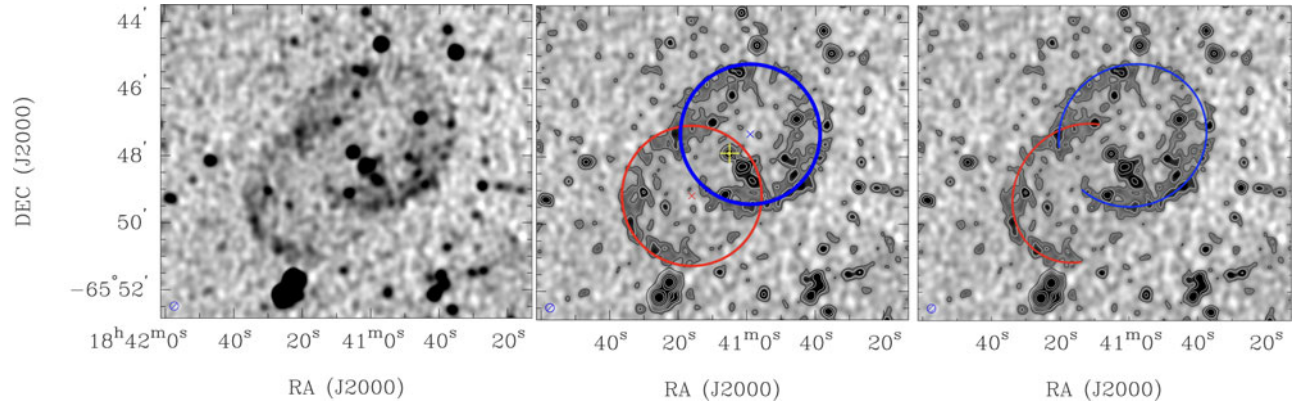


Figure 2. The double-shell structure of ORC J1841–6547 as seen in the deep ASKAP 944 MHz radio continuum images. Left: high-contrast greyscale image. – Middle: overlaid with radio contours at 0.05, 0.012, 0.25, 0.5, 1, 2, 5 and 10 mJy beam^{-1} and two coloured rings of 240″ diameter each. The ring centres are marked with crosses, while the central host galaxy is marked with a yellow plus sign. Right: similar to the middle image, but emphasising the partial and somewhat elongated nature of the shells. The image resolution (15”) is indicated in the bottom left corner of each panel. At the adopted host galaxy redshift of $z_{phot} \sim 0.18$, 1″ corresponds to ∼3 kpc.

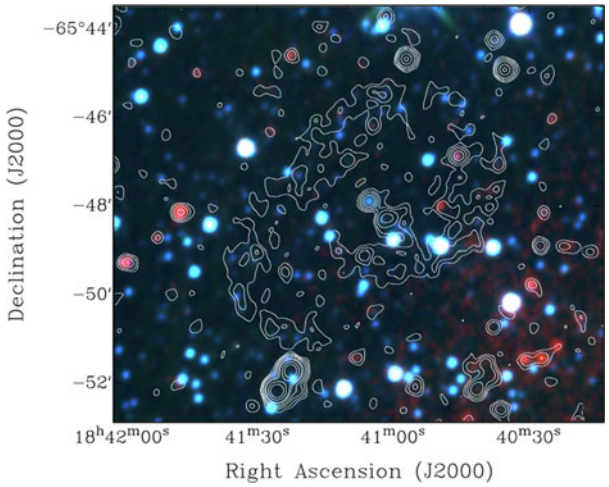


Figure 3. ASKAP 944 MHz radio continuum contours of ORC J1841–6547 overlaid onto an RGB colour image created from the WISE infrared bands. The image resolution and radio contour levels are as in Figure 2.

2024c, their Figure 6), is between ORCs 1 and 4, on the low-mass side of Pasini et al. (2022)’s brightest cluster radio galaxy sample (see also Veronica et al. 2026).

3.3. The jet-like emission

Radio continuum emission is also detected to the SW of the host galaxy (see Figure 4), extending over ∼70″. While two of the three likely companion galaxies (see Figure 5) are located within this emission patch, the radio peaks are offset from any galaxies. In particular, the brightest radio component (944 MHz peak at 18:41:01.3, –65:48:17, ∼30″ offset from the host galaxy) shows a wedge-shaped morphology resembling an inward moving shock. We note that the 1.4 GHz and 944 MHz peak positions are slightly offset; the respective peak fluxes are ∼0.7 and 0.9 mJy beam^{-1}. Deeper, high-resolution radio continuum images are needed to further analyse this extended structure, which may be the remnant of a jet emerging from the host galaxy.

3.4. Diffuse X-ray emission

We find a catalogued X-ray source, possibly associated with ORC J1841–6547, in both ROSAT (1WGA J1840.8–6546, White, Giommi, & Angelini 2000) at α, δ (J2000) = 18^h 40^m 50.3^s, –65° 46′ 38″ with a 0.2–2 keV energy of 1.53×10^{-13} erg s^{-1} cm^{-1} and eROSITA (1eRASS J184048.9–654700, Merloni et al. 2024) with 7.2×10^{-14} erg s^{-1} cm^{-1} in the 0.2–2.3 keV band. At the adopted redshift of $z = 0.18$ (or luminosity distance $D = 872$ Mpc) this corresponds to an X-ray luminosity of $L_X = 1.4 \times 10^{43}$ erg s^{-1} (ROSAT) and 6.6×10^{42} erg s^{-1} (eROSITA). The position uncertainty for the ROSAT detection is ∼1′ and for the 1eRASS position ∼10″, and the low count number statistics of the eRASS1 detection preclude robust judgement regarding its spatial extent. The target of the ROSAT pointed observations was the Seyfert galaxy ESO 103-G035 ($D = 58$ Mpc), at a projected distance of 28’ from the double-shell system.

Figure 6 shows the ROSAT PSPC X-ray emission contours overlaid onto our ASKAP 944 MHz radio continuum image. The X-ray emission appears to be elongated north-west to south-east, likely consisting of diffuse emission and compact sources. Interestingly, it coincides and partially fills the ORC’s north-western shell, while also overlapping with the host galaxy and the south-western radio extension. The position of the south-eastern X-ray maximum is ∼1′ offset from the host galaxy, coinciding with the radio south-eastern radio extension, while the north-eastern X-ray maximum has no obvious radio or optical counterparts. Deeper X-ray data are needed to confirm and further explore the morphology, extent and possible association of the hot gas with the ORC J1841–6547 radio shell system and its host galaxy.

Diffuse X-ray emission, when detected in galaxy groups, is nearly always centred on a luminous elliptical or lenticular galaxy (Mulchaey et al. 2003). Offset X-ray emission likely indicates group members in the process of merging as suggested for the nearby Physalis radio shell system (Koribalski et al. 2024c, see Section 4.2).

4. Comparison with other ORCs and radio shell systems

To inform the discussion in Section 5, we briefly compare the properties of ORC J1841–6547 to ORC J2103–6200 (ORC 1), ORC

https://doi.org/10.1017/pasa.2026.10193 Published online by Cambridge University Press

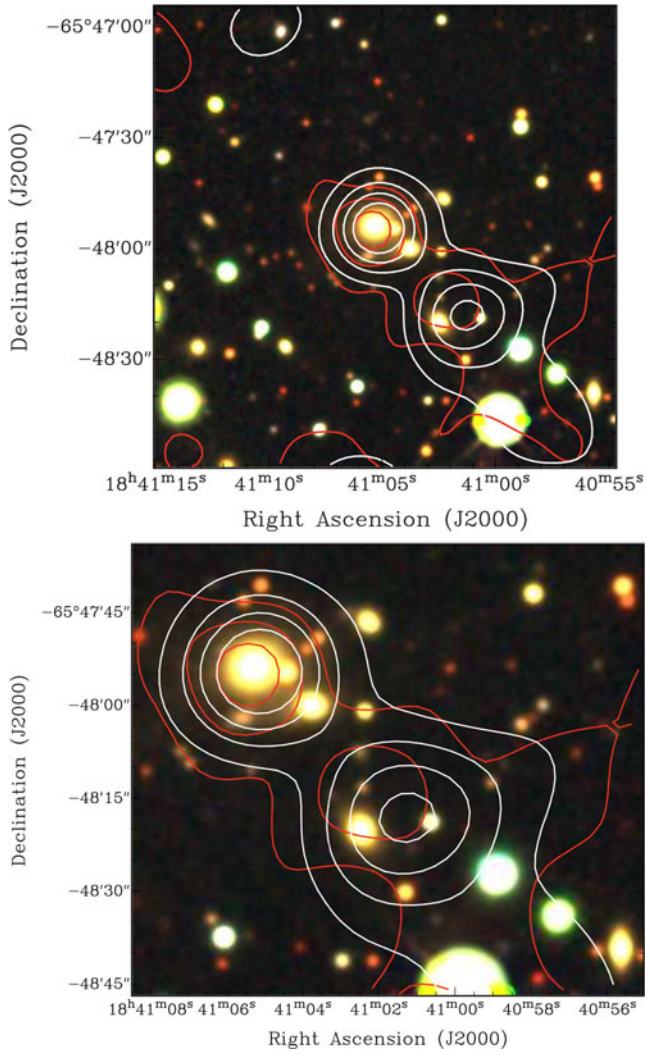


Figure 4. The inner region of ORC J1841–6547. DESI Legacy Survey DR10 optical RGB (*irg*-bands) image of the ORC J1841–6547 host galaxy and its surroundings overlaid with ASKAP radio contours at 944 MHz (white: 0.2, 0.4, 0.6 and 0.8 mJy beam^{-1}; 20″ resolution) and 1.4 GHz (red: 0.2, 0.4 and 0.6 mJy beam^{-1}; 20″ resolution). The top image is centred on the host galaxy, while the bottom image zooms in to the area SW of the host galaxy.

J1555+2726 (ORC 4) and ORC J0102–2450 (ORC 5), and nearby radio shell systems, Physalis and Cloverleaf.

4.1. Comparison to ORCs 1, 4 & 5

MeerKAT 1.3 GHz radio continuum images of ORCs 1, 4 and 5 are shown side-by-side in Figure 7, smoothed to 10″ resolution, highlighting similarities (size, edge-brightening, surface brightness, . . .) as well as differences (core brightness, internal structure, . . .) in their radio morphologies. Not included in this collage is the recently discovered MIGHTEE ORC (Norris et al. 2025a), whose angular size of 35″ is about a factor two smaller than that of ORCs 1, 4 and 5 (Norris et al. 2021b; Koribalski et al. 2021). All four odd radio circles have massive elliptical galaxies at their centres with redshifts of 0.55 (ORC 1), 0.45 (ORC 4), 0.27 (ORC 5) and 0.20 (MIGHTEE ORC), respectively. Deep optical images from the DESI Legacy Imaging Surveys (Dey et al. 2019) reveal several, less massive companion galaxies in their surroundings (based on their photometric redshifts), suggesting the central elliptical galaxy is a brightest group galaxy (BGG). The respective ORC group environments, including companions, are further explored in the review by Koribalski & Norris (in preparation).

Table 2. Properties of the ORC J1841–6547 host galaxy and associated galaxy group.

DESI DR10 position	$18^h\ 41^m\ 05.27^s$, −65° 47′ 53.6″
	280.27197°, −65.79823°
Galaxy names	DES J184105.27–654753.64
	2MASS J18410527–6547536
	2MASX J18410522–654753
	WISEA J184105.19–654753.8
	SMSS J184105.10–654753.7
Photometric redshifts	0.1248[a]
	0.1463[b]
	0.1795 ± 0.0052[c]
	0.1784[c]
Galaxy stellar mass[c]	3.1×10^{11} M$_\odot$
BCG-like galaxy[c]	Yes
R_{500c} radius[c,*]	0.603 Mpc
M_{500c} mass[c,*]	0.75×10^{14} M$_\odot$
MASS[d] K_s (mag)	14.45 ± 0.11 (profile fit)
	14.04 ± 0.1 (4″ aperture)
−> black hole mass	$\sim 4 \times 10^8$ M$_\odot$
WISE[e] W1,2,3,4 (mag)	13.71, 13.55, 12.73, >9.26
DESI DR10 *griz* [mag]	17.96, 16.74, 16.29, 15.97
ASKAP flux density	1.10 ± 0.02 mJy (944 MHz)
	0.75 ± 0.11 mJy (1.4 GHz)

References: (a) Bilicki et al. (2014), (b) Bilicki et al. (2016), (c) Wen & Han (2024), (d) Cutri et al. (2013) (e) profile fit, Wright et al. (2010), fluxes are possibly confused by two neighbouring sources. *Group properties.

The radio morphologies of the above ORCs all show edge-brightened radio rings, while ORC J1841–6547 consists of two partial rings. That said, the high-resolution MeerKAT 1.3 GHz image of ORC 1 by Norris et al. (2022) reveals complex internal structure, likely consisting of two or more rings/shells plus diffuse emission. Furthermore, the GMRT image of ORC 4 reveals a radio segment east of the primary ring, which was confirmed as a second, much fainter ring in the MeerKAT 1.3 GHz image shown by Riseley et al. (2024) and here in Figure 7. Projection effects need to be kept in mind, leading to different appearances of similar sources depending on the viewing angle. No secondary ring is seen in the MeerKAT 1.3 GHz image of ORC 5, which reveals a pronounced C-shape morphology. The SE companion to the ORC 5 host galaxy is prominently located in the midpoint of the C-shape, giving the structure a WAT-like appearance, while faint radio synchrotron threads exist just inside the western ring gap.

4.2. Nearby radio shell systems

Recently, two nearby radio shell systems were found in ASKAP radio continuum images, somewhat resembling the more distant ORCs. This allowed for detailed radio and follow-up X-ray studies. Both systems are characterised by multiple and/or nested radio shells surrounding a central elliptical BGG. The closest one is the Physalis system (ASKAP J1914–5433, Koribalski et al. 2024c) centred on ESO 184-G042 and its companion LEDA 418116,

https://doi.org/10.1017/pasa.2026.10193 Published online by Cambridge University Press

Table 3. Properties of the ORC J1841–6547 host galaxy and its brightest companion galaxies (c1, c2, and c3), based on their photometric redshifts by Wen & Han (2024), obtained from the DESI Legacy Imaging surveys DR10.

ORC J1841–6547	α, δ (J2000) position (deg, deg)	DESI DR10 g, r, i, z-band (mag)	WISE W1, W2 (mag)	Redshift z_{phot}	Log stellar mass ($M_\odot$)	Notes
Host galaxy	280.27197, –65.79823	17.728, 16.583, 16.175, 15.883	15.918 16.321	0.1795 ± 0.0052	11.492	BCG-like
c1	280.26562, –65.79999	19.361, 18.212, 17.808, 17.497	17.618, 18.050	0.1742 ± 0.0051	10.662	
c2	280.26019, –65.80558	19.234, 18.046, 17.618, 17.297	17.315, 17.721	0.1773 ± 0.0045	10.822	
c3	280.25940, –65.79623	20.464, 19.357, 18.983, 18.704	19.024 19.899	0.1884 ± 0.0069	10.065	

Table 4. ASKAP radio continuum flux densities for the components of ORC J1841–6547.

	1.4 GHz flux (mJy)	944 MHz flux (mJy)	α
Host galaxy	0.75 ± 0.11	1.13 ± 0.08	–1.0
Host + ext.	1.9 ± 0.3	3.2 ± 0.2	–1.3
NW shell (blue)	2.9 ± 0.4	8.7 ± 0.2	–2.8
SE shell (red)	1.3 ± 0.4	4.9 ± 0.2	–3.4
Total	~6	17.5 ± 0.5	–2.7

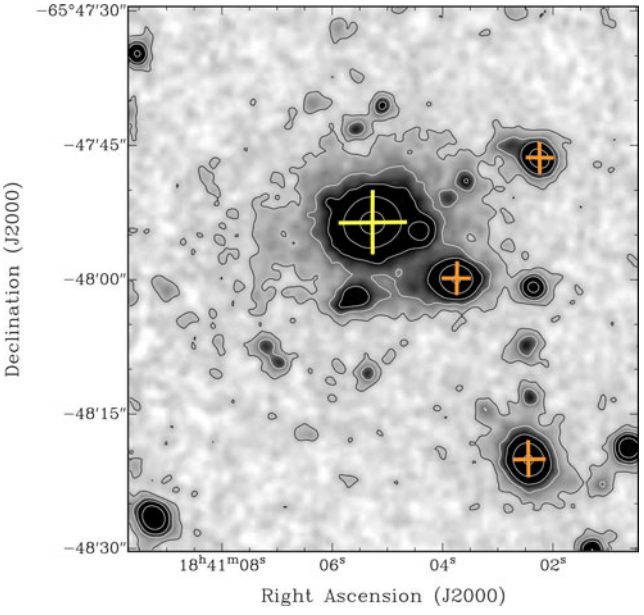


Figure 5. DESI Legacy Survey DR10 optical g-band image of the ORC J1841–6547 host galaxy (marked with a yellow cross) and surroundings. Three likely companion galaxies, based on their photometric redshifts (see Table 4), are marked with orange crosses. Diffuse stellar light is highlighted with a black contour while white contours show the brighter stellar bodies.

both elliptical galaxies, at a distance of only 75 Mpc (redshift $z = 0.017$). Physalis has a diameter of ~145 kpc and features a central radio ridge. Interestingly, our follow-up study with XMM-Newton reveals the X-ray emission to be offset from the radio ridge and centred on the companion galaxy. The second radio shell system is known as the Cloverleaf (ASKAP J1137–0050, Dolag et al. 2023, Koribalski et al., in prep.) centred on the elliptical galaxy CGCG 012-043 at a distance of ~200 Mpc (redshift $z = 0.046$), spanning 400 kpc. A follow-up XMM-Newton study by Bulbul et al. (2024) also shows the X-ray emission to be offset. In both cases, the hosts are massive elliptical galaxies surrounded by several companions, that is, they are BGGs. In their Physalis study, Koribalski et al. (2024c) find an example of such offset in Magneticum simulations and discuss possible shell formation mechanisms.

5. Discussion

We established that the host of ORC J1841–6547 is a massive elliptical galaxy which is surrounded by an envelope of diffuse stellar light, likely the signature of past merger activity, and at least three, much smaller companion galaxies. The host galaxy properties and environment (see Tables 2 and 3) are similar to those of other ORC host galaxies. Compact radio emission from the ORC host galaxies is detected, but varies in strength (see Figure 7). While no double-sided radio jets or lobes are observed, past activity of the host's supermassive black hole (SMBH) is likely, suggesting that the galaxy surroundings are filled with the fading (ageing) magnetised plasma of remnant lobes. The low radio surface brightness of ORC J1841–6547 and absence of active radio jets from the host galaxy suggests the shells are old, most likely relics or remnants left behind after the jet emission ceased (e.g. Komissarov & Gubanov 1994; Shabala et al. 2024). Their edge-brightened morphology strongly suggests that shocks are involved.

Overall, a number of physical processes are contributing to the ionised plasma in the CGM of massive elliptical galaxies. The CGM is a highly dynamic, time-variable environment, but not as turbulent as the intra-cluster medium. The apparent lack of radio jets from the central AGN of the ORC J1841–6547 host galaxy suggests it is currently inactive, but former recurring activity means that fossil radio-emitting plasma is present. Depending on the time since last activity, jet driven cavities may be present as well as fading radio lobes whose size, structure and appearance change with age. Stellar and starburst winds as well as turbulence may also be present, traceable via optical spectroscopy (e.g. Coil et al. 2024).

Furthermore, the evolution and growth of the massive host galaxy involves accretion and mergers, which on rare occasions drive powerful merger shocks into the CGM (Dolag et al. 2023). These shocks can have a wide range of Mach numbers. Once re-ignited by shock waves, the compressed fossil plasma may again become detectable at radio wavelengths (e.g. Enß lin & Brüggen 2002; Riseley et al. 2025). Quantifying the expected radio luminosity is difficult as shown by Böss et al. (2024) due to large uncertainties in CR acceleration efficiency models and magnetic field strength.

Riseley et al. (2025) present a detailed multi-wavelength study of the Hickson Compact Group (HCG) 15, in which no active jets or hotspots are detected from any of the five massive member galaxies. Instead, around galaxies HCG15-C (UGC 1620) and

https://doi.org/10.1017/pasa.2026.10193 Published online by Cambridge University Press

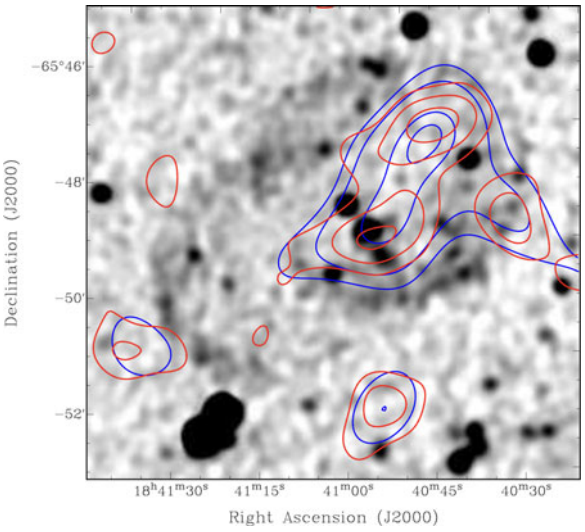


Figure 6. ROSAT PSPC X-ray contours overlaid onto the ASKAP 944 MHz radio continuum image (greyscale) of ORC J1841–6547. The ROSAT images were smoothed to 60" resolution (red contours) and 100″ resolution (blue contours), showing extended X-ray emission within the ORC's north-western shell and overlapping with the host galaxy and radio extension.

HCG15-D (UGC 1618) extended diffuse radio emission is present with radio powers of $P_{150\,\mathrm{MHz}} = (3.23 \pm 0.09) \times 10^{23}$ W Hz^{-1} and $P_{1\,400\,\mathrm{MHz}} = (2.22 \pm 0.02) \times 10^{22}$ W Hz^{-1}, consistent with that of steep-spectrum remnant radio sources (e.g. Riseley et al. 2022). Compared to galaxy clusters (e.g. Venturi et al. 2022), galaxy group environments are characterised by smaller number of galaxies, lower velocity dispersion, lower kinetic energy and less mergers. While merging clusters often show radio relics in their outskirts, created by cluster merger shocks (e.g. Brown 2011; van Weeren et al. 2019), the detected odd radio circles appear to be the result of merger shocks in galaxy groups.

ASKAP has shown to be highly suited to detecting LSB radio emission, for example, the ageing lobes of giant radio galaxies (Koribalski 2026) and steep-spectrum relic/remnants of unknown nature (e.g. Smeaton et al. 2025). In the following we explore the ORC environments (Section 5.1), discuss the radio power – mass relation (Section 5.2), re-energised remnant radio lobes (Section 5.3), precessing jets (Section 5.4), other double rings (Section 5.5) and consider ORC formation mechanisms (Section 5.6).

5.1. Galaxy group environment

The ORC host galaxies are massive elliptical galaxies surrounded by several companions, suggesting they are BGGs. While they resemble BCGs, their masses and number of companions are lower than for clusters. Galaxy groups typically host several large galaxies, which dominate the overall mass and luminosity, and many dwarf galaxies, which can be excellent tracers of the group dynamics, interactions and total mass. Groups dominated by spiral galaxies are typically gas-rich, see for example H I studies of the Hickson Compact Group (HCG) 44 (Serra et al. 2013) and the NGC 6221 group (Koribalski & Dickey 2004), while those dominated by elliptical galaxies, contain little gas. Osmond & Ponman (2004) find that most X-ray bright groups contain a bright central early-type galaxy and highlight the importance of elliptical BGGs. In a follow-up study of 30 nearby groups in their sample, Croston et al. (2005) find 19 (63%) to be associated with a AGN-related radio source, with roughly half of these in an active state (i.e. showing a double-lobed structure). Most of the currently inactive BGGs would have gone through periods of SMBH activity; their remnant lobes now either dispersed or only detectable in deep radio surveys. Although, Giacintucci et al. (2011) find that the intragroup medium (IGM) can confine such remnant lobes, preventing them from dissipating quickly.

An example of a remnant/relic radio galaxy is NGC 1534, studied in detail by Hurley-Walker et al. (2015) and Duchesne & Johnston-Hollitt (2019). It shows two fading lobes, spanning 600 kpc, with a very steep spectral index ($\alpha = -2.1 \pm 0.1$). The radio lobes are very diffuse with no signs of jets or hot spots. The host, NGC 1534, is a lenticular galaxy with a prominent dust lane (like NGC 5128) at a distance of 80 Mpc ($z_{\mathrm{spec}} = 0.017816$). It is the BGG of a loose group. Another example is the nearby NGC 507 galaxy group (Brienza et al. 2022), which shows the presence of diffuse radio emission with complex, filamentary morphology likely related to a previous outburst of the central galaxy. Here the remnant plasma has been displaced by the sloshing motions on large scales, likely caused by interactions between remnant plasma and the external medium.

In addition, the CGM filling the space between the currently inactive BGGs, which is mixed with the ageing electron plasma from remnant radio lobes, is also subject of dynamical processes driven by the still ongoing assembly of the groups. Simulations demonstrate that powerful merger shocks, for example, formed on rare occasions during the evolution of the BGG, will expand through the enriched CGM. This happens in an analogous way to that in galaxy clusters, but due to the lower density and temperature of the CGM this cannot be directly observed in X-rays as the counterparts in galaxy clusters. Thereby these shock waves are sweeping up and re-energising cosmic rays in the diffuse plasma, resulting in edge-brightened shells detected as radio rings, aka ORCs. A wide range of ORC sizes and morphologies can result in haloes of varying sizes. Figure 8 shows some examples for this scenario, compared to ORC 6. The middle panel shows an example for a Milky Way-sized halo, which underwent a triple merger event (see Dolag et al. 2023). The right panel shows a ten times more massive halo, undergoing a major merger event (see Ivleva et al. 2026). In such scenarios, various complex morphologies can appear, including double shells and nested shells. Interestingly, the shallower potential in a group-like environment together with the impact of AGN feedback can lead to more significant offsets between the X-ray bright CGM and the BCG (Koribalski et al. 2024c; Ivleva et al. 2026). Here, the X-ray bright CGM is sometimes centred on the impacted galaxy instead of the BGG. The Physalis ORC is the only one that is close enough to have very significant X-ray observations showing this offset (Koribalski et al. 2024c), while for Cloverleaf and ORC 6 they only have indications of an offset diffuse emission in X-rays.

5.2. Scaling relations

The location of ORC J1841–6547 (ORC 6) in the radio power versus total mass diagram, shown by (Koribalski et al. 2024c, their Figure 6), is between ORCs 1 and 4, on the low-mass side of Pasini et al. (2022)'s brightest cluster radio galaxy sample.

In Figure 9 we explore the scaling relation between the 1.4 GHz relic radio power and the X-ray luminosity for galaxy clusters and compare them to the three radio shell systems where X-ray data are available. We took the set of 39 galaxy clusters, which have been uniformly extracted from the NRAO VLA Sky Survey (NVSS) by

https://doi.org/10.1017/pasa.2026.10193 Published online by Cambridge University Press

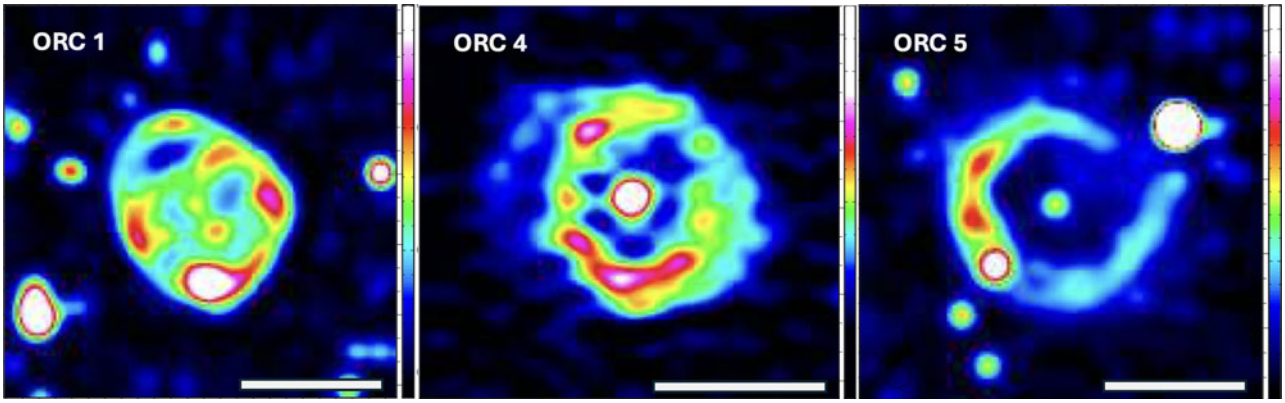


Figure 7. MeerKAT 1.3 GHz wide-band radio continuum images of ORC 1 (left, Norris et al. 2022), ORC 4 (middle, Riseley et al. 2024), and ORC 5 (right). While the ORCs have similar morphologies, the strength of the radio core varies substantially as well as the amount of diffuse emission between ring and core. The images are shown at 10″ resolution; the length of scale bar is 60″.

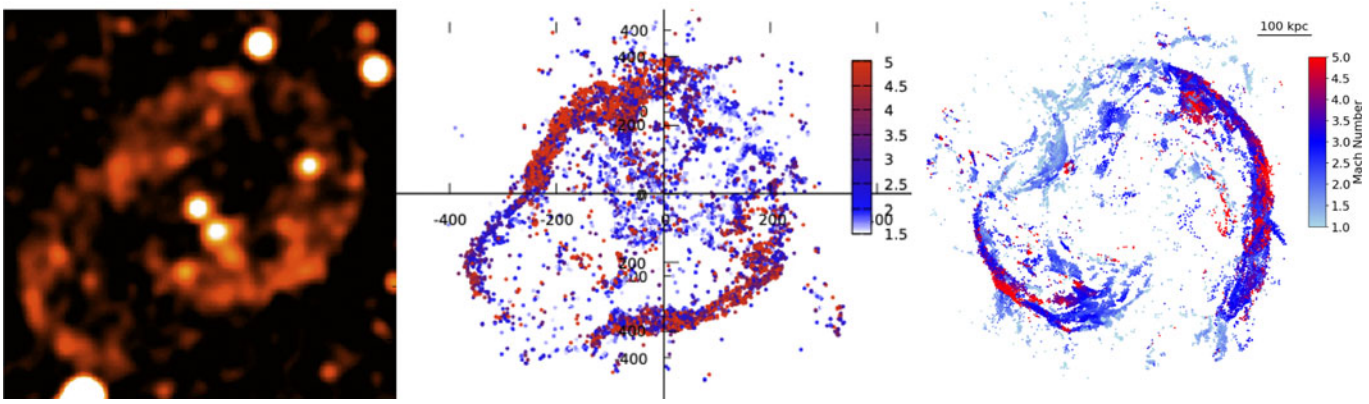


Figure 8. Left: ASKAP 944 MHz radio continuum image of ORC J1841–6547 (ORC 6). Middle and right: Simulated merger shocks from a MW galaxy like halo (middle, Dolag et al. 2023) and a ten times more massive halo (right, Ivleva et al. 2026), both selected to roughly match the morphology of ORC 6. The colour coding on the middle and right panels show the sonic Mach number determined by the shock finding algorithm (Beck, Dolag, & Donnert 2016).

Nuza et al. (2017). Some of the systems have several identified features (like double relics), which we then summed together to have a fair comparison to the total radio luminosity of the shells within the ORC systems. While the Physalis system seems to be in an early stage of the evolution within these systems, ORC 6 and the Cloverleaf system have comparable size and radio power than the relics in galaxy clusters, despite being much less massive. The similarity in size indicates that the shallower potential within the group environment, allows the powerful shocks to travel to relatively larger distances which in turn can make them more circular. In addition, reaching the same power despite being much less massive indicates that the relative contribution of the AGN activity foster much more effective conversion of the shock energy into radio emission, similar to the relatively larger impact of AGN feedback within groups compared to galaxy clusters.

Indeed, such a break from scaling relations for the ORCs' radio power is puzzling, particularly since the mass–radio halo power correlation seems to persist down group scales according to recent surveys (e.g. Cuciti et al. 2023; Stroe et al. 2025). This excess in radio brightness suggests that there must be a concurrence of several complex phenomena in the group environment – an assumption which is further validated by the rarity of ORCs. Interestingly, a recent systematic search for the diffuse emission in high redshift clusters indicated that bright outliers of these scaling relations are found when a large enough sample of sources is investigated (Di Gennaro et al. 2025). Also brightest cluster radio galaxies (see Pasini et al. 2022; Koribalski et al. 2024c) as well as emission of remnant radio lobes in low mass groups (for example NEST200047-D2, Brienza et al. 2022) are populating the intermediate region of radio luminosity while bridging the scales between clusters and ORC environments, and could potentially contribute to the overall picture.

In order to identify the necessary processes, simulations with appropriate models invoking several different mechanisms at play are necessary. So far, various numerical studies with varying complexity have investigated the possible impact of different mechanisms separately that have been proposed to take part, namely merger shocks (Dolag et al. 2023; Ivleva et al. 2026), AGN (e.g. Shabala et al. 2024) and stellar feedback (e.g. Coil et al. 2024). As already mentioned in Section 5.1, Ivleva et al. (2026) have recently explored the limits of purely shock-driven acceleration of cosmic ray electrons from the thermal pool, in a cosmological simulation of an assembling galaxy group. While producing fitting X-Ray luminosities and radio morphologies (c.f. Figure 8), the resulting radio luminosity at 150 was underestimated by a factor of about 1 000 compared to observed ORCs. As argued by the authors

https://doi.org/10.1017/pasa.2026.10193 Published online by Cambridge University Press

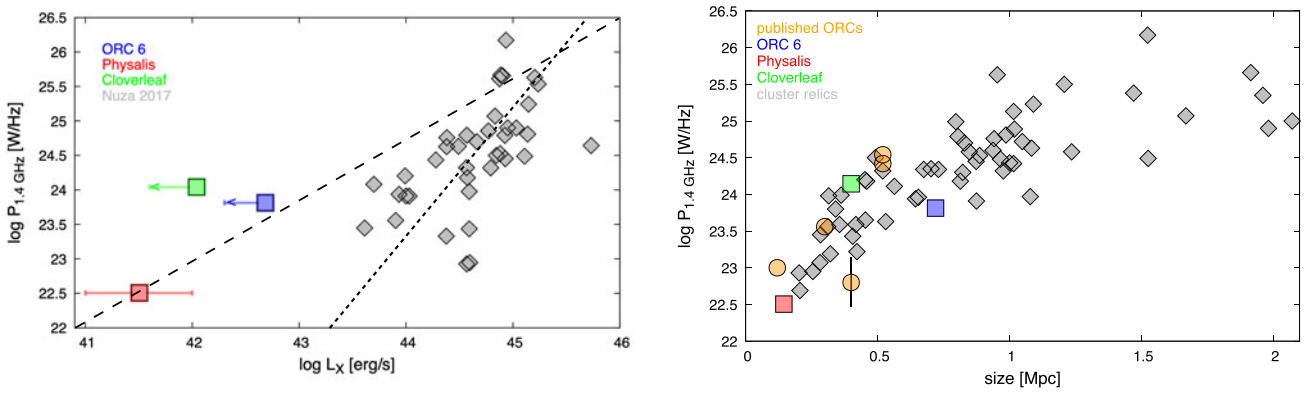


Figure 9. Scaling relation of 1.4 GHz radio power ($P_{1.4\,\mathrm{GHz}}$) versus X-ray luminosity (left) and size (right) for 39 NVSS-detected clusters with radio relics from Nuza et al. (2017) and for ASKAP-detected radio shell systems in three nearby galaxy groups. For the radio relics we use their catalogued NVSS 1.4 GHz flux densities and largest linear sizes (LLS) and show the slope of the corresponding scaling relation $P_{1.4\,\mathrm{GHz}} \propto L_X^{1.9}$ (derived from de Gasperin et al. 2014 using $L_X - M_{200}$ relation) with the dotted line. The dashed line shows a powerlaw relation with the slope 0.9 for visual guidance. For the radio shell systems, Cloverleaf (green; $D = 200$ Mpc), Physalis (red; $D = 75$ Mpc) and ORC 6 (blue, $D = 872$ Mpc), we use the measured 1.4 GHz flux densities of the radio shells and the respective ring/shell diameters. On the right side we added five known ORCs (orange) for which we have no X-ray detections. From smallest to largest these are: the MIGHTEE ORC, ORC 5, ORC J1027–4422 (uncertain redshift), plus ORCs 1 and 4. We use the respective MeerKAT 1.3 GHz images to measure their approximate ring fluxes.

of this study, the lower luminosity must be caused by two main effects, namely (i) an insufficient amount of relativistic electrons in the model and (ii) underestimated magnetic field strengths. The likely reason for (i) is the prescription of CR electron acceleration from the thermal pool. The electron acceleration efficiency η (i.e. the fraction of the dissipated shock energy that is available for CR electron acceleration) used in this work (based on Kang 2024) converges to a maximum value of $\eta \approx 10^{-4}$ in the regime of the detected shocks $\mathcal{M}_s \sim 3 - 5$. Recent plasma kinetic simulations by Gupta et al. (2024) find acceleration efficiencies a factor of three higher for Mach 5 than Kang (2024) and saturate at Mach 20 with efficiencies one order of magnitude higher. They consider more strongly magnetised shocks, however. To the best of our knowledge, no current plasma-kinetic simulation provides a sufficiently complete picture of CR electron acceleration efficiency in low Mach number, high beta shocks. The discrepancy in radio brightness can also be an implication for the existence of a considerable CR seed population in the environment of the sock, which is not modelled in that study. However, simply adding missing electron populations through AGN and stellar outflows would not explain the high radio luminosity according to Ivleva et al. (2026), as they estimate the total energy budget contributed by mergers versus AGN bubbles to be on the same order of magnitude (c.f. Discussion in their Section 4.2.) – leading to only a boost in radio power by a factor of two when adding AGN electrons, though an increase by three orders of magnitudes is necessary, within their modelling. Hence, the authors conclude that stronger magnetic fields are additionally required, which is also suggested by recent plasma simulations, predicting significant amplification of magnetic fields in the environments of cosmological shocks (e.g. Zhou et al. 2022, 2024).

Nevertheless, fossil cosmic ray electron populations must be included in realistic models of galaxy groups hosting ORCs, although the exact energy budget contributed by AGN remains an unresolved issue. Re-energisation by shocks of these sub-relativistic electrons would be possible, judging by the aforementioned high Mach numbers that a merger shock can trigger in the CGM (This has been studied in the case of ions by e.g. Caprioli, Zhang, & Spitkovsky 2018). Although ORC 6 does not display current signs of AGN activity, prior accretion events can not be ruled out, as the activity of AGN is known to be able to vary on timescales of 10–100 Myr (e.g. Shabala et al. 2008; Shulevski et al. 2015; Brienza et al. 2021). The diffuse stellar halo of ORC6's central elliptical galaxy is indicative of previous merger events, which might be triggers of the past AGN activity episodes.

A detailed radio and X-ray study of the Physalis system was carried out by Koribalski et al. (2024c), who measured total ASKAP 944 MHz and 1.4 GHz flux densities of at least 145 ± 2 and 79 ± 2 mJy, respectively. These correspond to radio powers of $P_{944\,\mathrm{MHz}} = 9.8 \times 10^{22}$ W Hz^{-1} and $P_{1.4\,\mathrm{GHz}} = 5.4 \times 10^{22}$ W Hz^{-1}. The Physalis radio shells were estimated to contain ~60% of the total radio flux, corresponding to 3.2×10^{22} W Hz^{-1} used in Figure 9. An analysis of new XMM-Newton X-ray data is underway (Khabibullin et al. in preparation).

5.3. Remnant radio lobes

The radio morphology of ORC J1841–6547 somewhat resembles that of nearly circular (fat) double-lobed radio galaxies such as Fornax A (Fomalont et al. 1989) but only the radio cocoon, created by the plasma backflow, is detected. Neither active inner jets nor hot spots are seen. While such remnant radio galaxies are quite common, their lobes are rarely edge-brightened or devoid of internal emission. But there is evidence for limb-brightening at the radio lobe boundaries (e.g. Carvalho et al. 2005; Daly et al. 2010) such that FR II lobes may indeed be radio hollow (Mathews & Guo 2012).

Simulations of the remnant lobe evolution of FR II-type radio galaxies by Shabala et al. (2024) show significant edge-brightening when re-energised by a plane-perpendicular shock wave. Alternately, merger shocks propagating outwards from the central galaxy (at rare occasions during its evolution) into remnant lobes will also re-ignite the magnetised plasma (for a study on the contribution of adiabatic compression of a fossil CR electron population in an AGN bubble see Wang & Heinz 2026). There may be consecutive merger shocks contributing to the radio brightness of the shells or bubbles during the growth of the central elliptical.

https://doi.org/10.1017/pasa.2026.10193 Published online by Cambridge University Press

This would alleviate some of the strain on the DSA acceleration efficiency. Theoretical models by Blasi (2004), and kinetic plasma simulations by Caprioli et al. (2018) can be simplified, such that the nomalisation of the spectrum resulting from re-acceleration is defined by the maximum of the number density of the seeds and newly energised particles, while the slope of the resulting total spectrum is the flatter between the slope of seed and newly energised populations. This can boost the luminosity of a system like NEST200047-D2 (Brienza et al. 2021) by one order of magnitude for a shock with a sonic Mach number of four, even without considering amplification of the magnetic field by the shock. However, a detailed study of this mechanism is beyond the scope of this work and warrants future studies.

On smaller scales, buoyant bubbles in 2D and 3D simulations (Churazov et al. 2001; O'Neill et al. 2009, respectively) expanding into the ICM can form vortex rings or torus-like features when viewed at or close to the jet axis (see also Brienza et al. 2021).

5.4. Precessing radio jets

Could the two rings of ORC J1841–6547 have been created by double-sided precessing jets emerging from the central galaxy? Geometrically, the time-integrated 3D structure of such a system would resemble a rim-brightened double cone with a wide opening angle, resembling an hour-glass slightly inclined to the line of sight. The latter looks like a single ring if viewed face-on. The peculiar radio extension SW of the host galaxy, shown in Figure 4, could be related to an active one-sided jet. If the two shells were from an episode of precessing jet activity, their brightness is surprisingly uniform. None of the simulated shape seen by Horton et al. (2020) resemble ORC J1841–6547.

In a recent paper, Nolting et al. (2023) present simulations of jet precession in radio galaxies to examine how they evolve over time and model their radio synchrotron emission. They find that the jet trajectories can become unstable due to their own self-interactions and lead to 'reorientation events', often observed as X-, S- and Z-shaped radio galaxies. Another cause of the change in the jet direction might be associated with the spin evolution of the accreting BH, and cosmological simulations tracking the spin evolution in a self-consistent manner show that rapid spin direction changes are not uncommon (Sala et al. 2024).

The synthetic radio intensity and spectral index maps (and movies) produced by Nolting et al. (2023) at different viewing angles can be used for comparison with high-resolution radio observations. ORC-like structures are seen when viewing the remnant radio emission of precessing jets approximately end-on, shortly after the jet power has been turned off. The low brightness, specific timing and viewing angle would make these very rare radio morphologies in agreement with observations. Nolting et al. (2023)'s 3D magneto-hydrodynamical simulations allow for both double and single ring morphologies. Polarisation maps would be of particular interest and should allow to distinguish this scenario from radio relics created by merger shocks (Dolag et al. 2023).

5.5. Similar double rings in ASKAP

High-resolution ASKAP radio continuum images from several large survey science projects are now available in CASDA. These include, for example, shallow images from the Rapid ASKAP Continuum Survey (RACS, McConnell et al. 2020; Duchesne et al. 2023) for the whole southern sky and up to northern declinations of ∼40° (15 min. integration time per field), and deep images from the on-going EMU project (Hopkins et al. 2025) for ∼50% of the southern sky (10 h integration time per field). While searching for ORCs we found several double ring systems, two of which are shown in Figure 10. ORC J2207–5806 is an unusual double ring source found in the EMU-PS (Norris et al. 2021a), and also noted by (Norris et al. 2025b, their Figure 14). The elliptical host galaxy has a redshift of $z_{\rm phot} = 0.578 \pm 0.050$. The radio extent of 1.2′ corresponds to 470 kpc. ORC J0518–5105 is another stunning double ring, with a size of ∼4′. At the host galaxy redshift of $z_{\rm phot} = 0.113 \pm 0.010$ this corresponds to ∼500 kpc.

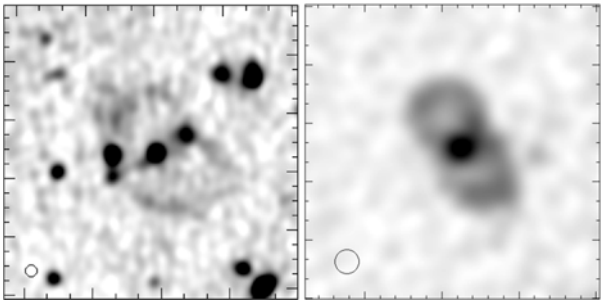


Figure 10. ASKAP radio continuum images of two double ring systems with a massive elliptical galaxy in their intersect region: ORC J0518–5105 (left) and ORC J2207–5806 (right). The respective image sizes are 10′ (left, 25″ resolution) and 2.5' (right, 12.5″ resolution).

5.6. Proposed ORC formation mechanism

The original ORC discovery papers (Norris et al. 2021b; Koribalski et al. 2021) presented possible formation scenarios, which are re-examined and updated with every new ORC detection (most recently, Koribalski et al. 2024b; Norris et al. 2025a). Numerical simulations of possible ORC formation mechanisms are essential to progress in this new field. Dolag et al. (2023) propose outwards moving merger shells as a likely mechanism to form ORCs with a wide range of radio morphologies, while (Nolting et al. 2023, see Section 5.4) look into precessing jets and Shabala et al. (2024) model the collision of a remnant lobe with an external shock.

A key feature of ORC J1841–6547 are its intersecting double radio shells reminiscent of remnant lobes where only the outer 'skin' (cocoon) remains. While faint, they look like two limb-brightened bubbles. Near circular double radio lobes like Fornax A are not uncommon, but generally filled with diffuse gas and rarely edge-brightened. There is some evidence that radio lobes may be hollow with backflow along the jet-forged cocoon.

Dolag et al. (2023) found outwards moving merger shells resembling ORCs in their high-resolution cosmological simulations of the evolution of massive elliptical galaxies and their CGM. Koribalski et al. (2024c) further expanded on this work, based on radio and X-ray observations of the nearby Physalis radio shell system, where merger shocks reignite remnant plasma within the group. ORC J1841–6547 may be a case where merger shocks expanding inside the cocoon of remnant radio lobes, here nearly perpendicular to the line of sight, result in the edge-brightened double shell morphology.

Double-double radio galaxies where re-started AGN jets propagate inside cocoons left behind by the initial jets, are used to infer the properties of the medium inside the cocoon (e.g. Kaiser, Schoenmakers, & Röttgering 2000; Yates, Shabala, & Krause 2018). Similarly, outwards moving merger shocks interact with

https://doi.org/10.1017/pasa.2026.10193 Published online by Cambridge University Press

the medium inside the cocoons, before becoming detectable as ORCs.

Future polarisation measurements will be crucial in estimating the likelihood of various formation scenarios for ORCs. So far, only two objects have been published with such an estimate, namely ORC 1 (Norris et al. 2022) and ORC J0356–4216 (Taziaux et al. 2025), which both display a degree of polarisation mostly between 10% and 20%. The merger shock simulation by Ivleva et al. (2026) predicts a slightly larger values around 20–40%, though the small discrepancy might well lie within observational uncertainties. Meanwhile, this model predicts spectral indices between 0.8 and 1.2 across the shock front. The two particular ORCs with polarisation measurements display the same edge-brightened rings with by flatter spectral indices at the outer rim, characteristic for shock acceleration. However, their spectrum seems to be a bit steeper than anticipated by Ivleva et al. (2026), which could be an indication of additional fossil cosmic ray populations present, similarly proposed by Shabala et al. (2024) based on their AGN driven re-acceleration simulations.

6. Conclusions

Our discovery of the double-shell system ORC J1841–6547 in deep ASKAP 944 MHz images adds diversity to the class of ORCs and prompted us to re-examine the proposed formation scenarios. The radio morphology of ORC J1841–6547 resembles that of two partial, intersecting shells with a massive elliptical galaxy, likely the system's host, in the centre of the intersect region. While the system looks somewhat like fat double-lobed radio galaxy, only the outlines of lobes or bubbles are seen, lacking the typical diffuse emission filling. Instead, we detect edge-brightened emission in the form of radio shells, not unlike radio relics in the outskirts of galaxy clusters (van Weeren et al. 2019; Mandal et al. 2020). The system spans 7′, that is, at least ∼1 Mpc at the host galaxy redshift (see Table 2). Each of the two shells/bubbles has a diameter of at least 540 kpc, similar to the size of ORC 1.

We propose that ORCs are radio relics around galaxy groups formed by outwards moving merger shocks during the evolution and growth of the central elliptical galaxy. Such relics are very rare and have not previously been noted in galaxy groups, while in galaxy clusters the occurrence of single or double radio relics in their outskirts is well established. Similar to clusters, the morphologies of radio relics around groups vary and depend on the properties of the IGM surrounding the central host galaxy. The ORC host galaxies have stellar masses of $\gtrsim 10^{11}$ $M_{\odot}$ and are notable as the brightest group galaxy (BGG). Our proposed formation scenario involves outwards moving merger shocks (Dolag et al. 2023) to re-energise the magnetised plasma from fading radio lobes via (a) re-acceleration of pre-existing fossil CR electrons and (b) in situ acceleration by an ensemble of shocks with different Mach numbers formed in the turbulent ICM. We expect the radio shells/relics to be highly polarised, which can be confirmed by deep radio observations. Deep X-ray and spectroscopic optical observations should be invaluable to reveal (possibly strongly disturbed) thermal gas content of the system as well as possible signatures of the dense warm gas and tidal distortions of the stellar bodies.

Acknowledgements. We thank the ASKAP team for their dedicated and continuing work on creating such a powerful survey telescope, together with a robust data processing pipeline and public archive. A big thank you also to Ian Heywood who processed the MeerKAT 1.3 GHz data of ORC 5, which we show in Figure 7 (right). We further thank Damiano Caprioli for inspiring discussions on CR acceleration.

KD, IK and AI acknowledge support by the COMPLEX project from the European Research Council (ERC) under the European Union's Horizon 2020 research and innovation programme grant agreement ERC-2019-AdG 882679. LMB is supported by NASA through grant 80NSSC24K0173 and NSF through grant AST-2510951.

This scientific work uses data obtained from Inyarrimanha Ilgari Bundara/the Murchison Radio-astronomy Observatory. We acknowledge the Wajarri Yamaji People as the Traditional Owners and native title holders of the Observatory site. CSIRO's ASKAP radio telescope is part of the Australia Telescope National Facility (https://ror.org/05qajvd42). Operation of ASKAP is funded by the Australian Government with support from the National Collaborative Research Infrastructure Strategy. ASKAP uses the resources of the Pawsey Supercomputing Research Centre. Establishment of ASKAP, Inyarrimanha Ilgari Bundara, the CSIRO Murchison Radio-astronomy Observatory and the Pawsey Supercomputing Research Centre are initiatives of the Australian Government, with support from the Government of Western Australia and the Science and Industry Endowment Fund.

This project used data obtained with the Dark Energy Camera (DECam), which was constructed by the Dark Energy Survey (DES) collaboration. Funding for the DES Projects has been provided by the U.S. Department of Energy, the U.S. National Science Foundation, the Ministry of Science and Education of Spain, the Science and Technology Facilities Council of the United Kingdom, the Higher Education Funding Council for England, the National Center for Supercomputing Applications at the University of Illinois at Urbana-Champaign, the Kavli Institute of Cosmological Physics at the University of Chicago, Center for Cosmology and Astro-Particle Physics at the Ohio State University, the Mitchell Institute for Fundamental Physics and Astronomy at Texas A&M University, Financiadora de Estudos e Projetos, Fundacao Carlos Chagas Filho de Amparo, Financiadora de Estudos e Projetos, Fundacao Carlos Chagas Filho de Amparo a Pesquisa do Estado do Rio de Janeiro, Conselho Nacional de Desenvolvimento Cientifico e Tecnologico and the Ministerio da Ciencia, Tecnologia e Inovacao, the Deutsche Forschungsgemeinschaft and the Collaborating Institutions in the Dark Energy Survey. The Collaborating Institutions are Argonne National Laboratory, the University of California at Santa Cruz, the University of Cambridge, Centro de Investigaciones Energeticas, Medioambientales y Tecnologicas-Madrid, the University of Chicago, University College London, the DES-Brazil Consortium, the University of Edinburgh, the Eidgenossische Technische Hochschule (ETH) Zurich, Fermi National Accelerator Laboratory, the University of Illinois at Urbana-Champaign, the Institut de Ciencies de l'Espai (IEEC/CSIC), the Institut de Fisica d'Altes Energies, Lawrence Berkeley National Laboratory, the Ludwig Maximilians Universitat Munchen and the associated Excellence Cluster Universe, the University of Michigan, NSF's NOIRLab, the University of Nottingham, the Ohio State University, the University of Pennsylvania, the University of Portsmouth, SLAC National Accelerator Laboratory, Stanford University, the University of Sussex, and Texas A&M University.

BASS is a key project of the Telescope Access Program (TAP), which has been funded by the National Astronomical Observatories of China, the Chinese Academy of Sciences (the Strategic Priority Research Program 'The Emergence of Cosmological Structures' Grant # XDB09000000), and the Special Fund for Astronomy from the Ministry of Finance. The BASS is also supported by the External Cooperation Program of Chinese Academy of Sciences (Grant # 114A11KYSB20160057), and Chinese National Natural Science Foundation (Grant # 12120101003, # 11433005).

The Legacy Survey team makes use of data products from the Near-Earth Object Wide-field Infrared Survey Explorer (NEOWISE), which is a project of the Jet Propulsion Laboratory/California Institute of Technology. NEOWISE is funded by the National Aeronautics and Space Administration.

The Legacy Surveys imaging of the DESI footprint is supported by the Director, Office of Science, Office of High Energy Physics of the U.S. Department of Energy under Contract No. DE-AC02-05CH1123, by the National Energy Research Scientific Computing Center, a DOE Office of Science User Facility under the same contract; and by the U.S. National

Science Foundation, Division of Astronomical Sciences under Contract No. AST-0950945 to NOAO.

Data availability statement. The ASKAP data products used in this article are available through CASDA. Additional data processing and analysis was conducted using the miriad software[b] and the Karma visualisation[c] packages. DESI images were obtained with the Legacy Survey SkyViewer.[d]

References

Bagchi, J., Durret, F., Neto, G. B. L., & Paul, S. 2006, Sci, 314, 791
Ballarati, B., et al. 1981, A&A, 100, 323
Beck, A. M., Dolag, K., & Donnert, J. M. F. 2016, MNRAS, 458, 2080
Bilicki, M., Jarrett, T. H., Peacock, J. A., Cluver, M. E., & Steward, L. 2014, ApJS, 210, 9
Bilicki, M., et al. 2016, ApJS, 225, 5
Blasi, P. 2004, APh, 21, 45
Böss, L. M., et al. 2024, A&A, 692, A232
Brienza, M., et al. 2021, NatAs, 5, 1261
Brienza, M., et al. 2022, A&A, 661, A92
Brown, S. D. 2011, JApA, 32, 577
Brüggen, M., et al. 2021, A&A, 647, A3
Bulbul, E., et al. 2024, A&A, 685, L2
Caprioli, D., Zhang, H., & Spitkovsky, A. 2018, JPPh, 84, 715840301
Carvalho, J. C., Daly, R. A., Mory, M. P., & O'Dea, C. P. 2005, ApJ, 620, 126
Churazov, E., Brüggen, M., Kaiser, C. R., Böhringer, H., & Forman, W. 2001, ApJ, 554, 261
Coil, A. L., et al. 2024, Natur, 625, 459
Croston, J. H., Hardcastle, M. J., & Birkinshaw, M. 2005, MNRAS, 357, 279
Cuciti, V., et al. 2023, A&A, 680, A30
Cutri, R. M., et al. 2013, Explanatory Supplement to the AllWISE Data Release Products. https://ui.adsabs.harvard.edu/abs/2013wise.rept....1C/abstract
Daly, R. A., et al. 2010, ApJS, 187, 1
de Gasperin, F., et al. 2014, MNRAS, 444, 3130
Dey, A., et al. 2019, AJ, 157, 168
Di Gennaro, G., et al. 2025, A&A, 695, A215
Dobie, D., et al. 2023, MNRAS, 519, 4684
Dolag, K., Böss, L. M., Koribalski, B. S., Steinwandel, U. P., & Valentini, M. 2023, ApJ, 945, 74
Duchesne, S. W., & Johnston-Hollitt, M. 2019, PASA, 36, e016
Duchesne, S. W., et al. 2023, PASA, 40, e034
Duchesne, S. W., et al. 2024, PASA, 41, e026
Enßlin, T. A., & Brüggen, M. 2002, MNRAS, 331, 1011
Ferrari, C., Govoni, F., Schindler, S., Bykov, A. M., & Rephaeli, Y. 2008, SSRv, 134, 93
Filipović, M. D., et al. 2022, MNRAS, 512, 265
Fomalont, E. B., Ebneter, K. A., van Breugel, W. J. M., & Ekers, R. D. 1989, ApJ, 346, L17
Giacintucci, S., et al. 2011, ApJ, 732, 95
Gupta, N., et al. 2024, PASA, 41, e027
Gupta, N., et al. 2025, PASA, 42, e099
Gürkan, G., et al. 2022, MNRAS, 512, 6104
Hopkins, A., et al. 2025, PASA, 42, e071
Horton, M. A., Krause, M. G. H., & Hardcastle, M. J. 2020, MNRAS, 499, 5765
Hotan, A. W., et al. 2021, PASA, 38, e009
Hurley-Walker, N., et al. 2015, MNRAS, 447, 2468
Hurley-Walker, N., et al. 2017, MNRAS, 464, 1146
Ivleva, A., Böss, L. M., Dolag, K., Koribalski, B. S., & Khabibullin, I. 2026, A&A, 706, A80

[b] https://www.atnf.csiro.au/computing/software/miriad/.
[c] https://www.atnf.csiro.au/computing/software/karma/.
[d] https://www.legacysurvey.org/viewer/.

Jarrett, T. H., et al. 2017, ApJ, 836, 182
Johnston, S., et al. 2008, ExA, 22, 151
Jones, A., et al. 2023, A&A, 680, A31
Kaiser, C. R., Schoenmakers, A. P., & Röttgering, H. J. A. 2000, MNRAS, 315, 381
Kang, H. 2024, JKoAS, 57, 155
Komissarov, S. S., & Gubanov, A. G. 1994, A&A, 285, 27
Koribalski, B., & Dickey, J. M. 2004, MNRAS, 348, 1255
Koribalski, B. S. 2012, PASA, 29, 359
Koribalski, B. S. 2022, in 2022 3rd URSI Atlantic and Asia Pacific Radio Science Meeting (AT-AP-RASC), 1–4
Koribalski, B. S. 2026, PASA, 43, e012
Koribalski, B. S., et al. 2021, MNRAS, 505, L11
Koribalski, B. S., et al. 2004, AJ, 128, 16
Koribalski, B. S., et al. 2020, Ap&SS, 365, 118
Koribalski, B. S., et al. 2024a, MNRAS, 533, 608
Koribalski, B. S., et al. 2024b, MNRAS, 531, 3357
Koribalski, B. S., et al. 2024c, MNRAS, 532, 3682
Koribalski, B. S., et al. 2026, PASA, 1–16
Mandal, S., et al. 2020, A&A, 634, A4
Mathews, W. G., & Guo, F. 2012, ApJ, 755, 13
McConnell, D., et al. 2020, PASA, 37, e048
Merloni, A., et al. 2024, A&A, 682, A34
Mulchaey, J. S., Davis, D. S., Mushotzky, R. F., & Burstein, D. 2003, ApJS, 145, 39
Nolting, C., Ball, J., & Nguyen, T. M. 2023, ApJ, 948, 25
Norris, R. P., et al. 2025a, MNRAS, 537, L42
Norris, R. P., et al. 2011, PASA, 28, 215
Norris, R. P., et al. 2021a, PASA, 38, e046
Norris, R. P., et al. 2021b, PASA, 38, e003
Norris, R. P., et al. 2022, MNRAS, 513, 1300
Norris, R. P., et al. 2025b, PASA, 42, e124
Nuza, S. E., Gelszinnis, J., Hoeft, M., & Yepes, G. 2017, MNRAS, 470, 240
O'Neill, S. M., De Young, D. S., & Jones, T. W. 2009, ApJ, 694, 1317
Osmond, J. P. F., & Ponman, T. J. 2004, MNRAS, 350, 1511
Pasini, T., et al. 2022, A&A, 661, A13
Riseley, C. J., et al. 2022, MNRAS, 515, 1871
Riseley, C. J., et al. 2024, A&A, 686, A44
Riseley, C. J., et al. 2025, A&A, 697, A45
Sala, L., Valentini, M., Bi_, V., & Dolag, K. 2024, A&A, 685, A92
Segal, G., et al. 2023, MNRAS, 521, 1429
Serra, P., et al. 2013, MNRAS, 428, 370
Shabala, S. S., Ash, S., Alexander, P., & Riley, J. M. 2008, MNRAS, 388, 625
Shabala, S. S., et al. 2024, PASA, 41, e024
Shulevski, A., et al. 2015, A&A, 583, A89
Smeaton, Z. J., et al. 2025, PASA, 42, e119
Stroe, A., et al. 2025, ApJ, 984, 24
Taziaux, S., et al. 2025, A&A, 702, A219
van Weeren, R. J., et al. 2019, SSRv, 215, 16
Velović, V., et al. 2022, MNRAS, 516, 1865
Venturi, T., et al. 2022, A&A, 660, A81
Veronica, A., et al. 2026, PASA, 43, e001
Wang, Y., & Heinz, S. 2026, arXiv e-prints, arXiv:2602.12479
Wen, Z. L., & Han, J. L. 2024, ApJS, 272, 39
White, N. E., Giommi, P., & Angelini, L. 2000, VizieROnline Data Catalog: The WGACAT version of ROSAT sources (White+ 2000), VizieR Online Data Catalog: IX/31. Originally published in: Laboratory for High Energy Astrophysics (LHEA/NASA), Greenbelt (2000)
Wright, E. L., et al. 2010, AJ, 140, 1868
Yates, P. M., Shabala, S. S., & Krause, M. G. H. 2018, MNRAS, 480, 5286
Zhou, M., Zhdankin, V., Kunz, M. W., Loureiro, N. F., & Uzdensky, D. A. 2022, PNAS, 119, e2119831119
Zhou, M., Zhdankin, V., Kunz, M. W., Loureiro, N. F., & Uzdensky, D. A. 2024, ApJ, 960, 12

https://doi.org/10.1017/pasa.2026.10193 Published online by Cambridge University Press